

**Supplementary Information for “Curvature Sensing by Cardiolipin in Simulated Buckled Membranes”**

Federico Elías-Wolff,<sup>1,2</sup> Martin Lindén,<sup>3</sup> Alexander P. Lyubartsev,<sup>2</sup> and Erik G. Brandt<sup>2</sup>

<sup>1</sup>*Department of Biochemistry and Biophysics, Stockholm University, Stockholm, Sweden*

<sup>2</sup>*Department of Materials and Environmental Chemistry, Stockholm University, Stockholm, Sweden*

<sup>3</sup>*Department of Cell and Molecular Biology, Uppsala University, Uppsala, Sweden<sup>a)</sup>*

(Dated: 19 October 2018)

---

<sup>a)</sup>Present address: Scania CV AB, Södertälje, Sweden

## S.1. AUTOCORRELATION TIME

We present detailed autocorrelation analysis for the allPE simulations. The autocorrelation time depends on lipid diffusion, so we expect these results to be reasonable approximations for the lipids in all simulated systems. The autocorrelation time  $t_{\text{ac}}$  is defined as twice the exponential decay time<sup>1</sup>,

$$t_{\text{ac}} = 2t_{\text{exp}} = 2 \int_0^{\infty} dt \tilde{C}(t), \quad (\text{S.1})$$

where  $\tilde{C}(t)$  is the normalized autocorrelation function of each  $\hat{\rho}_i$ -bin in a one-component system,

$$C(t) = (\langle \hat{\rho}_i(t' + t)\hat{\rho}_i(t') \rangle - \langle \hat{\rho}_i \rangle^2) / (\langle \hat{\rho}_i^2 \rangle - \langle \hat{\rho}_i \rangle^2), \quad (\text{S.2})$$

averaged over all  $M$  bins and  $N = 512$  lipids.  $\hat{\rho}$  is the single lipid midplane distribution, i.e.,  $\hat{\rho}_i(t) = 1$  if the lipid in question occupies bin  $i$  at time  $t$ , and  $\hat{\rho}_i(t) = 0$  otherwise (for a one-component bilayer,  $\langle \hat{\rho}_i \rangle \approx 1/M$ ). From Fig. S.1b, we determine that the lipid autocorrelation time is  $t_{\text{ac}} = 2t_{\text{exp}} \approx 124\text{ns}$ .

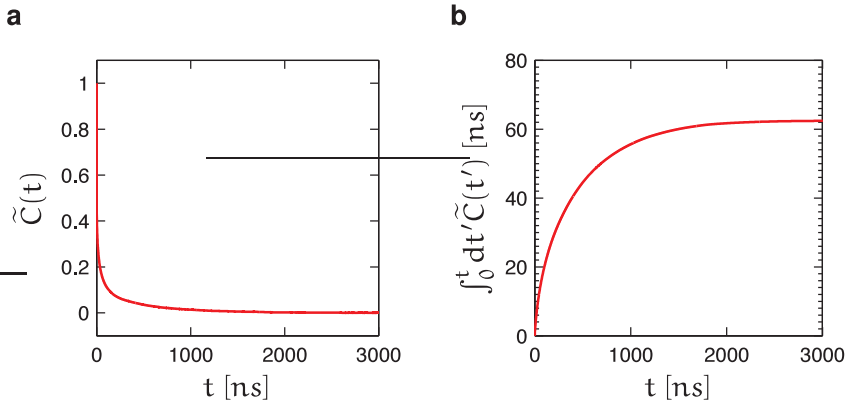


FIG. S.1. a: Normalized autocorrelation function  $\tilde{C}(t)$ . b: The exponential decay time,  $t_{\text{exp}} = \int_0^{\infty} dt' \tilde{C}(t')$ . The autocorrelation time is  $t_{\text{ac}} = 2t_{\text{exp}} \sim 124\text{ns}$ . Data from the allPE simulation.

## S.2. LIPID COMPONENT DISTRIBUTIONS

Here we present the densities  $\rho_j(s)$  for each lipid component  $j$ , which are used to compute the relative densities  $\phi_j(s)$  in Eq. (2) in the main text. These densities are computed

by constructing histograms of the innermost tail bead positions for each lipid while discarding the initial 1  $\mu\text{s}$  as equilibration. The  $\rho_j(s)$  are normalized as probability densities to facilitate comparison.

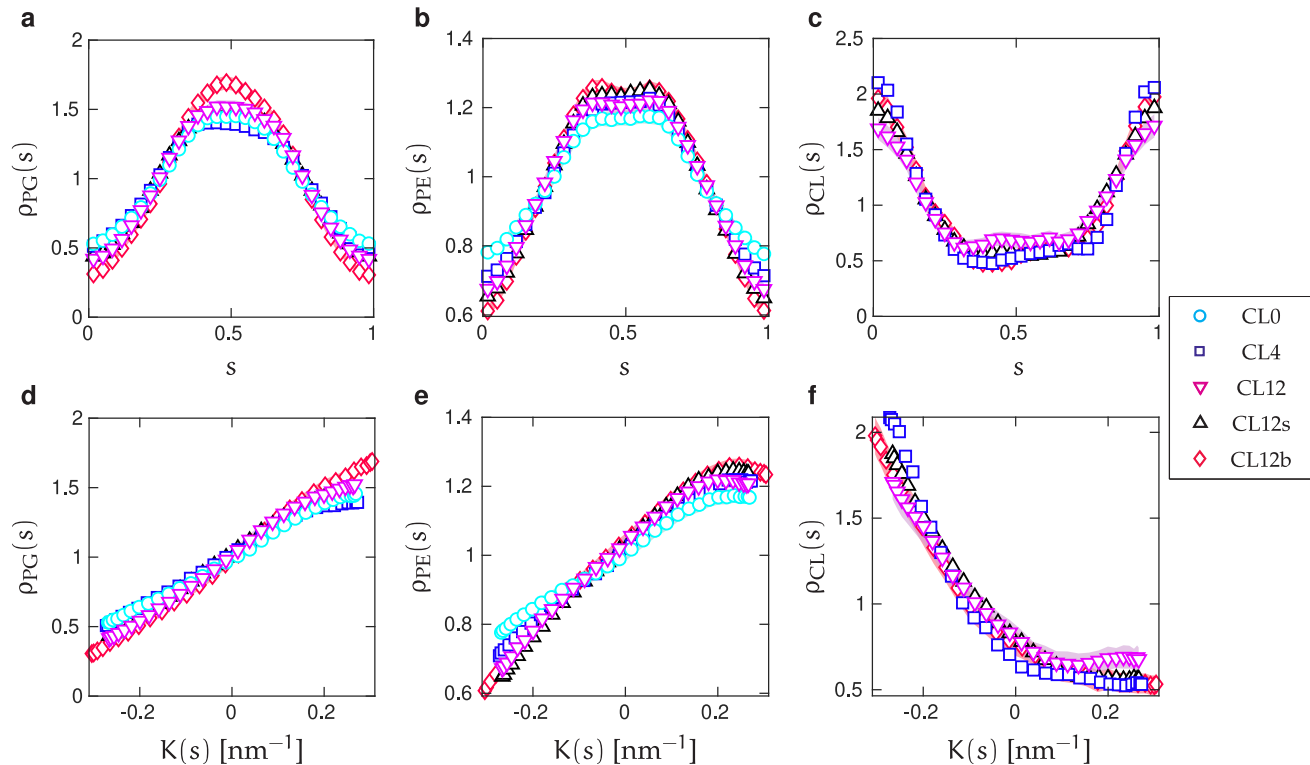


FIG. S.2. Densities,  $\rho_j(s)$ , for each lipid component as functions of  $s$  (panels a–c) and of  $K(s)$  (panels d–f). Panel (a,d) corresponds to POPG, (b,e) to POPE, and (c,f) CL. Symbols correspond to each of the simulations listed in Table 1 in the main text, and shaded areas to the standard error of the mean, shown only for the CL0, CL12 and CL12b systems.

### S.3. LIPID DISTRIBUTION ALONG THE BUCKLED BILAYER

Here we show the  $(x, z)$ -densities for the innermost tail-beads and the head-beads for each lipid component in the CL12 simulation. In addition to depicting the results in Fig. S.2 in a more intuitive albeit less quantitative form, we notice that while the planes formed by the head-beads of POPE and CL are both at 2.1 nm from the midplane (blue and red solid curves in Fig. S.3), the distance for POPG is slightly larger at 2.3 nm (dashed green curves in Fig. S.3).

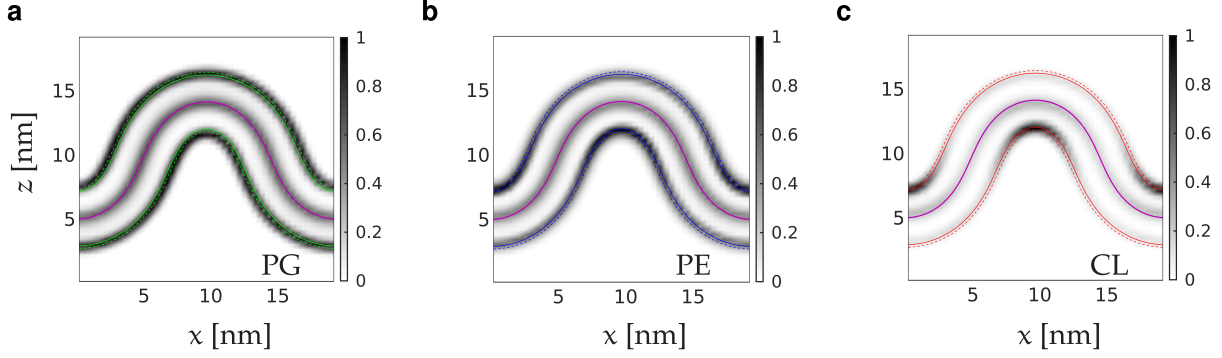


FIG. S.3.  $xz$ -density plots of head- and tail-beads for each lipid component in the CL12 simulation. The head bead count is multiplied by 4 for POPG and POPE, and by 8 for CL, since for every head bead there are two and four tail beads, respectively, and the midplane contains tail beads from both monolayers. The purple curve corresponds to the average fitted midplane, i.e.  $(X(\langle\gamma\rangle), Z(\langle\gamma\rangle))$ . The outer curves are parallel to the first one, separated by 2.1 nm (solid lines), and by 2.3 nm (dashed lines). Green curves correspond to POPG, blue to POPE and red to CL. Data from the CL12 simulation.

#### S.4. ION DISTRIBUTION

Here we present  $(x, z)$ -density plots for the ions in the CL0, CL12 and CL12s simulations. The first two systems contain only counterions (128  $\text{Na}^+$  ions distributed along the bilayer surface). The CL12s simulations contain additionally 207  $\text{Cl}^-$  ions, and corresponding  $\text{Na}^+$  ions, yielding a total of 335  $\text{Na}^+$  ions. We observe that  $\text{Na}^+$  ions distribute along the bilayer surface, while  $\text{Cl}^-$  ions localize away from the bilayer.

#### S.5. ENHANCEMENT RATIO

Here, we give a detailed derivation of Eq. (9) in section III E in the main text. We consider a 3-component lipid mixture, and write again the free energy per monolayer as

$$F = L_y L \int_0^1 ds \tilde{\rho}(s) \sum_{j=1}^3 \left( \frac{\phi_j(s)}{2} M_j (K(s) - K_j)^2 + k_B T \phi_j(s) (\log \phi_j(s) - 1) \right), \quad (\text{S.3})$$

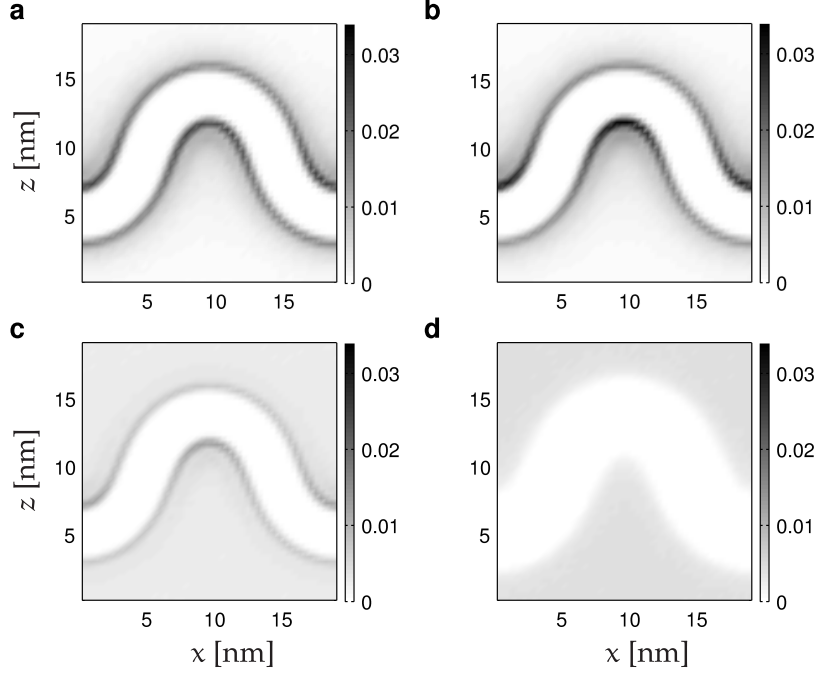


FIG. S.4. Ion distribution in the  $(x, z)$ -plane. Panels (a,b) correspond to the CL0 and CL12 simulations, with only counterions, which in both cases correspond to 128  $\text{Na}^+$  ions. Panels (c,d) correspond to the CL12s simulation, which contains 335  $\text{Na}^+$  ions (shown in panel c) and 207  $\text{Cl}^-$  ions (panel d).

where  $\phi_j(s)$  denotes the local mole fraction of lipid species  $j$ . Equation (S.3) is subject to the constraints

$$\int_0^1 ds \tilde{\rho}(s) \phi_j(s) = n_j, \quad (\text{S.4})$$

which fix the number  $n_i$  of lipids of species  $i$  in the monolayer and the additional constraint

$$\sum_{i=1}^3 \phi_i(s) = 1, \quad (\text{S.5})$$

which ensures point-wise normalization of the molar fractions. Minimizing Eq. (S.3) with respect to  $\phi_i(s)$ , leads to

$$-k_B T \log \phi_j(s) = \frac{M_j}{2} (K(s) - K_j)^2 + \mu_j + \alpha(s), \quad (\text{S.6})$$

where  $\mu_j$  is a Lagrange multiplier (chemical potential) from enforcing condition (S.4), and  $\alpha(s)$  is a function that acts to enforce the point-wise constraint (S.5). We find

$$e^{\alpha(s)} = \sum_{j=0}^3 e^{-\mu_j - \frac{M_j}{2}(K(s) - K_j)^2}. \quad (\text{S.7})$$

The same point in  $s$  opposing monolayers has the same curvature with opposing sign ( $K_{\text{upper}}(s) = -K_{\text{lower}}(s)$ ). Thus, considering both monolayers yields

$$\log \frac{\phi_i^+(s)}{\phi_i^-(s)} = \frac{2}{k_B T} K(s) (K_i M_i) + \mu_i^+ - \mu_i^- - (\alpha^+(s) - \alpha^-(s)). \quad (\text{S.8})$$

Since the monolayers are symmetric the chemical potentials are the same.  $\alpha(s)$  is however not symmetric across the bilayer, but fortunately it does cancel for expressions of relative fractions ( $\log(\phi_i/\phi_j)$ ). Thus, we finally arrive at the relation

$$\log \frac{\phi_i^+(s)\phi_j^-(s)}{\phi_i^-(s)\phi_j^+(s)} = 2K(s) \frac{K_i M_i - K_j M_j}{k_B T}. \quad (\text{S.9})$$

## S.6. ADDITIONAL SUPPLEMENTARY FIGURES

Here we show a detailed version of Fig. 3d, where we depict the standard errors for each curve as a shaded area on separate panels.

## REFERENCES

<sup>1</sup>B. A. Berg and A. Billoire, *Markov chain Monte Carlo simulations* (Wiley Online Library, 2008).

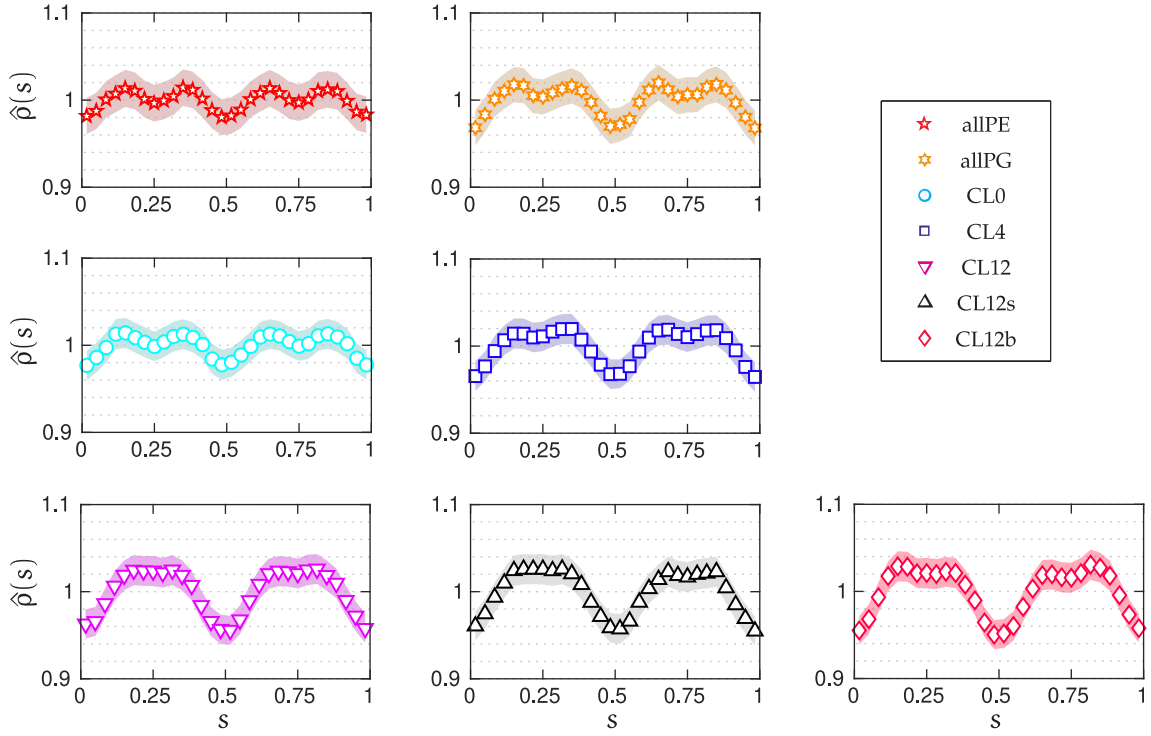


FIG. S.5. Same as Fig. 3d in the main text, but showing each curve in a different panel, and where the shaded areas correspond to the SEM for each system, which were omitted for clarity in Fig. 3d.